ACS Catalysis

Research Article

pubs.acs.org/acscatalysis

CO Oxidation Activity at Room Temperature over Au/CeO_2 Catalysts: Disclosure of Induction Period and Humidity Effect

Shuo Zhang,[†,‡] Xiao-Song Li,[†,‡] Bingbing Chen,[†,‡] Xiaobing Zhu,*[,†,‡] Chuan Shi,*[,†,‡] and Ai-Min Zhu[†,‡]

[†]Center for Hydrogen Energy and Liquid Fuels, [‡]Laboratory of Plasma Physical Chemistry, Dalian University of Technology, Dalian 116024, China

Supporting Information

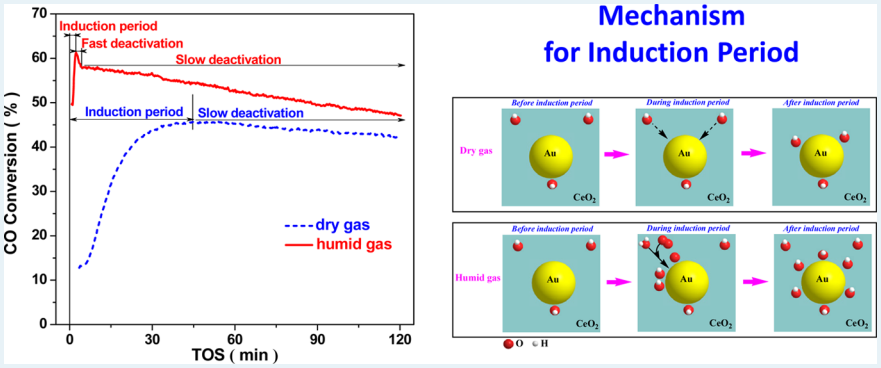

ABSTRACT: CO oxidation at room temperature over the Au/CeO_2 catalyst was investigated, of which the induction period arising from unreduced cationic Au was disclosed. The effect of humidity in reactant stream on catalyst activity was investigated during induction and deactivation periods. The induction period was significantly reduced from 44.8 min in dry stream to 3.3 min in wet stream containing 0.58 vol % of H_2O. The induction period was slightly shortened by further increasing water concentration in the reactant stream. The maximum initial activity was achieved with a wet stream containing 0.74 vol % of H_2O vapor. In situ DRIFTS measurements suggested that humidity contributed to the formation and consumption of reaction intermediates $[COOH]_s$ and hence enhanced the initial activity. After the induction period, the deactivation phenomena of Au/CeO_2 catalyst at varied rates under both wet and dry streams were observed. In contrast to a slow deactivation under dry stream, a fast deactivation in wet stream was first observed due to rapid blockage of active sites by water adsorption, followed by a slow deactivation rate due to gradual formation of surface carbonate species over catalyst with time on stream. A mechanism was proposed to illustrate the existence of induction period under both wet and dry streams.

KEYWORDS: *Au/CeO_2 catalyst, CO oxidation, induction period, humidity effect, initial activity, catalyst deactivation*

1. INTRODUCTION

Metal-oxide-supported gold nanoparticles have driven increasing research efforts because of their high catalytic activity, in order to understand their fundamental physicochemical properties. Catalytic activity of gold nanoparticles relates to particle size and shape, oxide support materials, coordination between gold nanoparticle and support, and so forth.[1−4] Investigations of the CO oxidation reaction for CO removal appear to be blooming due to various environment and energy applications on indoor air treatment, automotive emission control, and hydrogen fuel cells,[5] among others. The humidity effect on CO oxidation is closely related to individual supported Au system, especially the support materials used. Efforts have been made to investigate the humidity effect on CO oxidation over Au/Fe_2O_3, Au/CeO_2, Au/Al_2O_3, Au/TiO_2, Au/TiO_2–In_2O_3, and $Au/Ti(OH)_4$ catalysts.[6−14]

Metal-oxide-supported gold catalysts for CO oxidation possess an intrinsic advantage over other catalysts; however, inevitably, they tend to deactivate with time on stream (TOS) or during storage.[15−23] Two main reasons account for the catalyst deactivation: (1) carbonate accumulation leading to a reversible deactivation and (2) agglomeration of Au particles resulting in an irreversible deactivation. In recent studies, it was demonstrated that the deactivation is closely related to the buildup of carbonate species rather than an irreversible sintering of Au nanoparticles.[18−22,24] The presence of water has a positive effect to alleviate catalytic activity loss on Au/Fe_2O_3[18] and Au/Al_2O_3[19] catalysts, which is attributed to the conversion of carbonate species to less stable bicarbonate species. However, water may have a different effect on the activity of gold catalysts supported on a different metal oxide. For example, Au/TiO_2[13,23] and Au/In_2O_3–TiO_2[13] catalysts suffer from a loss of activity in the presence of water, which is

Received: December 30, 2013
Revised: August 21, 2014
Published: August 26, 2014

   dx.doi.org/10.1021/cs500614f | ACS Catal. 2014, 4, 3481−3489

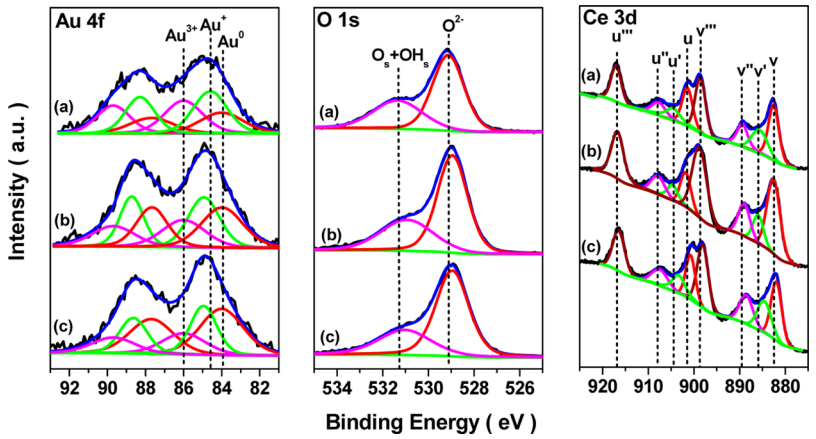

Figure 1. XPS spectra of Au 4f, O 1s, and Ce 3d of Au/CeO_2 catalyst: (a) before CO oxidation in dry stream, (b) after CO oxidation in dry stream, and (c) after CO oxidation in wet stream containing 0.74 vol % of H_2O.

attributed to loss of active sites occupied by excessive water molecules.

Among most of those studies, gas chromatography (GC) was employed to measure TOS concentration of CO and CO_2, which requires relatively long time to analyze samples. Due to long sample analysis interval, the dynamic response of initial activity during the induction period was not disclosed. In our recent work, it has been found that formaldehyde oxidation on the Au/CeO_2 catalyst in wet air exhibited a short induction period. Because CO oxidation at room temperature is attractive for various environmental applications, in this paper, we studied the induction period of CO oxidation over Au/CeO_2 catalyst at room temperature, and we investigated the humidity effect on catalyst activity during induction period and deactivation period, by activity evaluation and in situ DRIFTS measurements. In order to facilitate the observation of induction period and catalyst deactivation, the experiments were conducted at a high WHSV of 300 000 $mL{\cdot}h^{-1}{\cdot}g^{-1}$ and with CO conversion less than 100%. A rapid-response CO_x analyzer was employed online to measure the rapid change in CO and CO_2 concentration. A mechanism is proposed to illustrate the existence and difference of induction period under both wet and dry streams.

2. EXPERIMENTAL SECTION

2.1. Catalyst Preparation. Au/CeO_2 catalyst was prepared by deposition−precipitation method with urea, as described in our previous work.[24] Five grams of commercial CeO_2 powder (Rare-Chem Hi-Tech Co., Ltd. (RCC), China) were first added into 11 mL of aqueous $HAuCl_4{\cdot}4H_2O$ solution (10 $g{\cdot}L^{-1}$), further dispersed into 200 mL deionized (DI) water, and lastly, mixed with 0.16 M urea ($CO(NH_2)_2$) to form a slurry. After the mixture was stirred at 80 °C for 8 h and aged at room temperature for 12 h, the formed slurry was filtered and washed with DI water until neutral. The filtered cake was dried at 80 °C for 6 h and then calcined at 300 °C for 1 h under a synthetic air (20 vol % O_2 balance N_2) to obtain the fresh catalyst.

2.2. Catalyst Characterization. The Au loading on Au/CeO_2 catalyst was determined by inductively coupled plasma-atomic emission spectroscopy (ICP-AES, Optima 2000DV, U.S.A.). Specific surface area measurement was performed by BET method using nitrogen adsorption−desorption at −196 °C (NOVA2200e, Quantachrome Corporation, U.S.A.). All samples were degassed at 300 °C for 3 h prior to the measurements. Surface chemical states of Au/CeO_2 catalysts were characterized by X-ray photoelectron spectroscopy (XPS, ESCALAB250 Thermo VG, U.S.A.) using an Al Kα X-ray source (1486.6 eV) operated at 15 kV and 300 W. The binding energy was calibrated according to the XPS peak at carbon 1s at 284.6 eV. High-resolution transmission electron microscopy (HRTEM) micrographs were obtained with a Tecnai G2 20 S-TWIN microscope and operated at 200 kV.

The redox behavior was evaluated by temperature-programmed reduction (TPR) technique with Chemisorption Analyzer (Autochem II 2920, Micromeritics, U.S.A.). TPR experiments were performed using a gas mixture of 10 vol % H_2 balance Ar, at a flow rate of 50 $mL{\cdot}min^{-1}$, a temperature ramping rate of 10 $°C{\cdot}min^{-1}$ from 40 to 800 °C. The catalyst (80 mg) was pretreated in dry air at 300 °C for 1 h before each TPR experiment.

2.3. Catalytic Activity Evaluation. Catalytic activity evaluation was performed in a quartz U-tube reactor with inner diameter of 4 mm, surrounded by water bath at 20 ± 1 °C under ambient pressure. Prior to the reaction, 80 mg of catalyst was first mixed with 40 mg of quartz sand and then loaded into the quartz U-tube reactor. After the catalyst was treated with synthetic air at 300 °C for 1 h, a gas mixture containing 500 ppm of CO, 20 vol % O_2 balance N_2, was introduced into the reactor at a WHSV of 300 000 $mL{\cdot}h^{-1}{\cdot}g^{-1}$. Water vapor was carried by N_2 or O_2 through a water bubbler at room temperature. Water concentration was measured online using a dew point hygrometer (653−2, Testo, Germany), which is expressed as absolute humidity. Inlet and outlet gaseous products were online analyzed by a rapid-response CO_x analyzer (S710, Sick/Maihak, Germany). CO conversion, X_{CO}, was calculated as follows:

$$X_{CO}(\%) = \frac{C_{CO}^{in} - C_{CO}^{out}}{C_{CO}^{in}} \times 100 \quad (1)$$

where C_{CO}^{in} and C_{CO}^{out} represent the concentrations of CO in inlet and outlet gases, respectively. Because the CO concentration is only around 500 ppm, the temperature increase in catalyst bed arising from the exothermic reaction is negligible.

2.4. In Situ DRIFTS Analysis. Infrared spectra were recorded by an FTIR spectrometer (Tensor 27, Bruker, Germany) equipped with a liquid N_2 cooled Mercury−Cadmium−Telluride (MCT) detector. Scans were collected from 4000 to 1000 cm^{-1} at a resolution of 4 cm^{-1}. Catalyst samples were placed in a DRIFTS cell equipped with CaF_2 windows and pretreated in 20 vol % O_2 balance He at 300 °C for 1 h prior to DRIFTS experiments. Typical gas mixture was 2000 ppm of CO, 20 vol % oxygen balance helium. Water vapor was carried into the gas mixture by helium through a bubbler in a water bath at room temperature. After a designated amount of time, the CO flow was switched to a humid stream containing 0.74 vol % water, 20 vol % oxygen balance helium.

3. RESULTS

3.1. Catalyst Characterization. Au loading on Au/CeO_2 catalyst was 0.95 wt % as measured by ICP analysis. BET

dx.doi.org/10.1021/cs500614f | ACS Catal. 2014, 4, 3481−3489

Table 1. XPS Analysis of Au/CeO_2 Catalyst before and after CO Oxidation in Dry and Wet Streams

	peak position (eV)					proportion (at. %)				
catalyst	Au^0	Au^{1+}	Au^{3+}	O^{2-}	O_s+OH_s	Au^0/Au^a	Au^{1+}/Au^a	Au^{3+}/Au^a	$(O_s+OH_s)/O^b$	Ce^{3+}/Ce^c
fresh	84.0	84.6	86.0	529.1	531.3	25	40	35	37	20
used (dry)	84.0	84.9	86.0	529.0	531.0	37	36	27	35	23
used (wet)	84.0	85.0	86.0	529.0	531.1	48	31	21	32	20

$^a Au = Au^0 + Au^{1+} + Au^{3+}$ $^b O = O^{2-} + O_s + OH_s$ $^c Ce = Ce^{3+} + Ce^{4+}$

surface areas for CeO_2 and Au/CeO_2 catalyst were 79 and 82 $m^2 \cdot g^{-1}$, respectively.

XPS analysis was performed to investigate the chemical state of Au/CeO_2 catalysts before and after CO oxidation in dry and wet stream. The spectra of Au 4f, O 1s and Ce 3d XP for all three samples are shown in Figure 1. The main XPS results are summarized in Table 1. For quantitative evaluation, the XP spectra of the Au 4f signals were fitted by three different states, with binding energies of 84.0, 84.6, and 86.0 eV, respectively. The typical binding energies of Au $4f_{7/2}$ at 84.0 and 86.0 eV are assigned to Au^0 and Au^{3+}, respectively.[25−27] The assignment of the peak at 84.6 eV seems a little paradoxical in literatures.[27−36] Behm et al. assigned this peak to Au^0 in very small neutral Au cluster, whose binding energy is up-shifted due to particle size effects.[27] However, many studies reported the existence of interaction between Au and CeO_2 surface that involves a charge transfer from Au to CeO_2, leading to the formation of Au^+.[28−30] Hence, we adopted the assignment of the peak at 84.6 eV to Au^{1+}.[31−36] From Table 1, it is clearly shown that, in Au/CeO_2 catalyst before or after CO oxidation, Au existed in the mixed oxidation states of Au^0, Au^{1+}, and Au^{3+}. For fresh catalysts, the atomic ratios of Au^0, Au^{1+}, and Au^{3+} to the total surface Au species were 25%, 40%, and 35%, respectively. However, after CO oxidation in dry stream, the concentration of Au^{3+} and Au^{1+} decreased, although that of Au^0 increased to 37%. Similarly, after CO oxidation in wet stream, the change in oxidation state of Au followed the same tendency as that in dry stream, but considerably more Au^{3+} and Au^{1+} were reduced to Au^0 (48%). In addition, the peak at 84.6 eV shifted to higher binding energy after reaction, which may be related to the change in Au^{1+} concentration. The XPS results suggested that in situ reduction of cationic Au occurred during the CO oxidation at room temperature in both dry and wet streams.

Further information can be obtained from the O 1s spectra in Figure 1. Two types of oxygen species were distinguished by deconvolution of the O 1s spectra. The peak with binding energy at 529.1 ev is related to the lattice oxygen (O^{2-}), whereas the peak at 531.3 eV is associated with surface oxygen and/or surface hydroxyl species (O_s + OH_s).[25,37] As shown in Table 1, the peak deconvolution results indicate that the amount of surface oxygen and hydroxyl species is reduced after reaction. The existence of surface oxygen species is related to the coexistence of Ce^{3+} and Ce^{4+} in Au/CeO_2 catalyst, as evidenced by the Ce 3d XPS results shown in Figure 1 and Table 1. Due to the presence of Ce^{3+} in CeO_2 lattice, oxygen vacancies are formed. O_2 can adsorb on the vacancies, which reduces surface Gibbs energy, balances surface charge, and forms surface active oxygen species.

As shown in Figure 1, the Ce 3d spectra of Au/CeO_2 can be resolved into eight peaks, which is in accordance with many studies.[10,35,38−41] The assignment of each component peak is defined in Figure 1. The symbols of V and U represent the spin−orbit coupling of $3d_{5/2}$ and $3d_{3/2}$, respectively. The Ce $3d_{5/2}$ peaks are marked as v (882.5 eV), v″ (889.4 eV) and v‴ (898.6 eV) corresponding to the Ce^{4+} state, whereas that denoted as v′ at 885.6 eV is assigned to Ce^{3+}, implying that Ce exists in mixed valence states in Au/CeO_2 catalysts.[10,26] For the fresh catalysts, the proportion of Ce^{3+} to total surface Ce on Au/CeO_2 catalyst was 20%. For the used catalysts, the concentration of Ce^{3+} under dry and wet conditions were 23% and 20%, respectively, indicating that there is no obvious difference among the three catalysts.

Figure 2 shows H_2-TPR profiles of CeO_2 and Au/CeO_2 catalysts. Two peaks appear at the temperature ranging from 40 to 800 °C in the TPR profile of CeO_2 (Figure 2a), which are consistent with previous observations in literatures.[35,42] The peaks at 747 and 479 °C represent the reduction of bulk oxygen and surface capping oxygen of ceria, respectively. Besides the low temperature peak at 479 °C, a characteristic shoulder at 363 °C is likely due to formation of nonstoichiometric Ce oxides (CeO_x, x ranging from 1.9 to 1.7, or the β phase).[43] Compared with that of cerium oxide, the peak related to the reduction of surface oxygen of ceria, shifts downward to 79 °C in Au/CeO_2 catalyst (Figure 2b). This significant decrease in reduction temperature implies that the presence of gold facilitates the reduction of surface oxygen species.

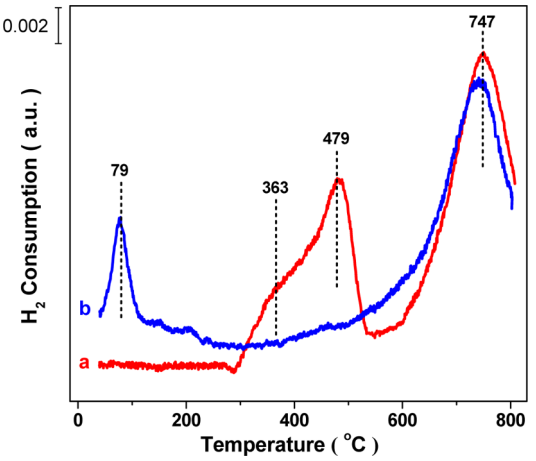

Figure 2. H_2-TPR profiles of (a) CeO_2 and (b) Au/CeO_2.

In summary, the shoulder peak at 363 °C and the main peak at 479 °C are both ascribed to the reduction of surface oxygen species generated from the structural defects of CeO_2. As mentioned above, surface oxygen species can be formed on the oxygen vacancies due to the presence of Ce^{3+} in CeO_2 lattice. These kinds of surface oxygen species can be easily reduced at temperature lower than 500 °C.[35,42,43] In addition, the reduction of lattice oxygen in CeO_2 needs higher temperature. For instance, the peak at 747 °C is ascribed to the reduction of Ce^{4+} to Ce^{3+}. Further reduction of Ce^{3+} cannot happen within the range of testing temperature.

dx.doi.org/10.1021/cs500614f | ACS Catal. 2014, 4, 3481−3489

3.2. Humidity Effect on Catalytic Activity during Induction and Deactivation Periods. The water concentration in dry stream was determined to be about 300 ppm by a dew point hygrometer, and those in wet streams are given in Figures 3, 4, 6, and 7 for each experiment. The CO oxidation

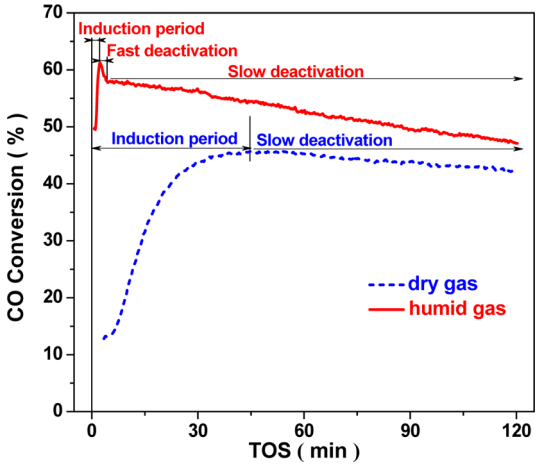

Figure 3. CO conversion versus time on stream (TOS) over Au/CeO_2 catalysts at 20 °C under dry stream and wet stream (containing 0.74 vol % of H_2O), with 500 ppm of CO/20 vol % O_2/N_2, and WHSV = 300,000 $mL{\cdot}h^{-1}{\cdot}g^{-1}$.

evaluation at room temperature was simulated with a CO concentration of 500 ppm, a level considered to be practical in some polluted air.

Figure 3 shows CO conversion with time on stream under dry and wet conditions. Generally, CO conversion shows two stages as the induction and deactivation periods. Once the stream entered the reactor, Au/CeO_2 catalyst started to be activated and reached maximum CO conversion, which is defined as initial activity. The time period before reaching the initial activity is defined as the induction period, and the time after reaching the initial activity is the deactivation period.

In dry stream, the catalyst underwent a long induction period of 44.8 min before reaching the maximum 46% of CO conversion. In contrast, the induction period was shortened to 2.3 min in a wet stream containing 0.74 vol % of H_2O and achieved 61% of CO conversion. After the induction period under wet stream, CO conversion exhibited a rapid decrease in the next few minutes to 58%, and then a slow decrease thereafter, in contrast to no fast deactivation stage under dry stream. Worth noting is that during the slow deactivation period, the decrease rate of CO conversion in wet stream (with 0.74 vol % of H_2O) was faster than that in dry stream, but the CO conversion in wet stream was still 5% higher than in dry stream after 120 min on stream (46% vs 41%). The faster deactivation in wet stream is attributed to faster consumption of [COOH]s species, as will be discussed later. Similar phenomena were also observed under wet streams with other water concentrations such as 0.58, 0.79, and 0.97 vol %.

Theoretically, if water is discontinued as a short induction period just finished, the fast deactivation might disappear. However, it is hard to test this idea with our current equipment setup. Even if the water supply is stopped right after the induction period, it would take a certain amount of time to equilibrate the gas system, and thus make it very hard to monitor the rapid change in activity timely.

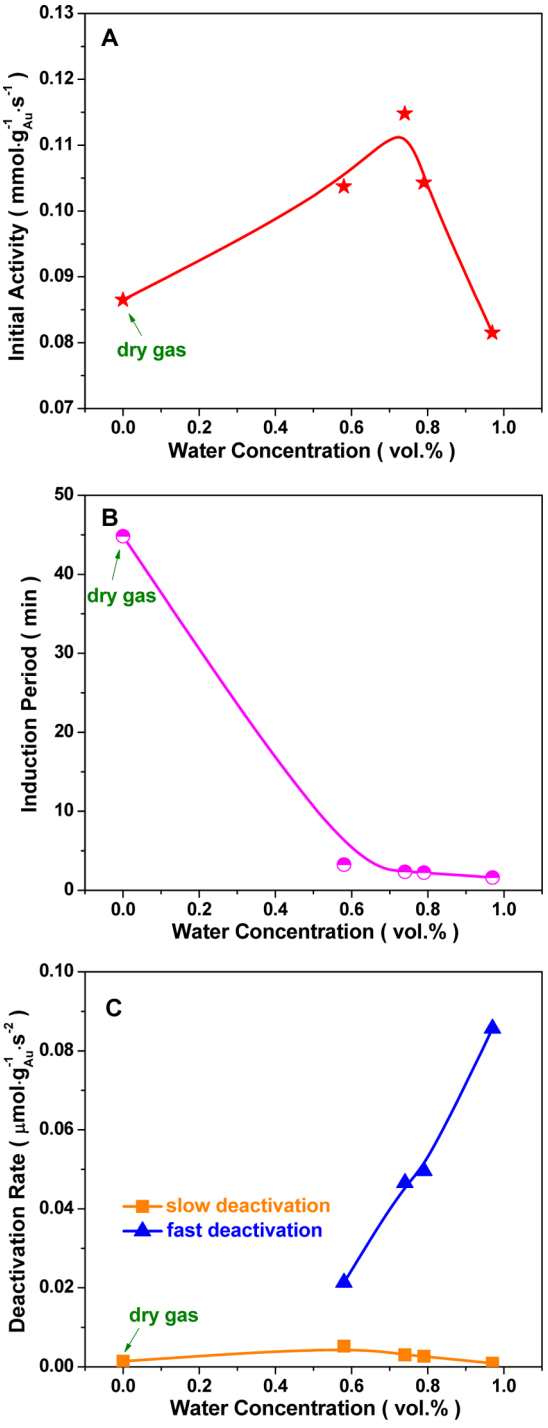

Figure 4. Dependence of (A) initial activity, (B) induction period, and (C) deactivation rate of Au/CeO_2 catalyst for CO oxidation at 20 °C on water concentration.

Figure 4 shows the initial activity, induction period and deactivation rate of Au/CeO_2 catalyst as a function of water concentration. Initial activity is expressed as a specific rate at a time of t_i,

$$\text{initial activity}\ (\text{mmol}{\cdot}\text{g}_{\text{Au}}^{-1}{\cdot}\text{s}^{-1}) = \frac{F{\cdot}C_{\text{CO}}^{\text{in}}{\cdot}X_{\text{CO}}^{t=t_i}}{m_{\text{Au}}} \quad (2)$$

where t_i is the moment ending the induction period or reaching maximum CO conversion, F is the total flow rate, $X_{\text{CO}}^{t=t_i}$ is the

dx.doi.org/10.1021/cs500614f | ACS Catal. 2014, 4, 3481−3489

CO conversion at t_i, and m_{Au} is the mass of Au on Au/CeO_2 catalyst. As shown in Figure 4A, the highest initial activity was obtained with ~0.74 vol % of H_2O.

Figure 4B clearly shows the effect of moisture on shortening the induction period. The induction period was significantly reduced from 44.8 min with dry stream to 3.3 min with wet stream containing 0.58 vol % of H_2O. Further increase in water content up to 0.97 vol % only resulted in a slight decrease in induction period from 3.3 to about 2 min.

Deactivation rate is defined as

$$\text{deactivation rate } (\mu\text{mol}\cdot g_{Au}^{-1}\cdot s^{-2}) = \frac{F\cdot C_{CO}^{in}\cdot(X_{CO}^{t=t_1} - X_{CO}^{t=t_2})}{t_2 - t_1} \quad (3)$$

where $X_{CO}^{t=t_1}$ and $X_{CO}^{t=t_2}$ represent CO conversion at two different times t_1 and t_2, respectively. In terms of wet condition, two deactivation stages (fast and slow) existed. For instance, during fast deactivation stage, t_1 equals t_i with initial activity, and t_2 can be the time at turning point (donated as t_{TP}) between fast and slow deactivation stages. However, during slow deactivation stage, t_1 equals $t_{TP,}$ and t_2 can be t_{TP} plus 60 min. By contrast, in terms of dry condition, t_1 equals to t_i with initial activity, and t_2 can be t_i plus 60 min. As shown in Figure 4C, the deactivation rates at slow deactivation stage under wet and dry conditions were much lower than that at fast deactivation stage. In wet stream, the deactivation rate at fast deactivation stage rapidly increased with water concentration, whereas that at slow deactivation stage only declined slightly with increasing water concentration. During fast deactivation stage under wet condition, the increase in deactivation rate with water concentration is ascribed to an elevated loss of active sites occupied or blocked by excess of water molecules.[42,44]

3.3. In Situ DRIFTS Measurements. *3.3.1. Formation of Intermediates.* Figure 5 shows in situ DRIFT spectra of Au/CeO_2 catalyst exposed to 2000 ppm of CO/He at 20 °C. Table 2 summarizes the IR bands assigned to $[COOH]_s$, carbonate, and water species in the literature. The bands at 1580, 1373, and 1418 cm^{-1} on Au/CeO_2 catalysts are ascribed to $\nu_{as}(OCO)$, $\nu_s(OCO)$, and $\delta(OH)$ of $[COOH]_s$, respectively. The band at 1288 cm^{-1} is associated with $\nu_{as}(OCO)$ of bidentate carbonate species, whereas the bands at 1445 and 1490 cm^{-1} are assigned to monodentate carbonate.[10,45−48] Interestingly, once Au/CeO_2 catalyst was exposed to 2000 ppm of CO, $[COOH]_s$ species was formed in the absence of water and O_2, which indicates that CO directly reacts with surface hydroxyl on Au/CeO_2 catalyst to form $[COOH]_s$ intermediates. This is consistent with the existence of hydroxyl species on Au/CeO_2 catalyst, as detected by DRIFTS (see Figure S1). The existence of hydroxyl groups was further confirmed by CO temperature-programmed surface reaction (TPSR) profiles in Figure S2. Starting from 100 °C, H_2 was produced owing to water−gas-shift (WGS) reaction between CO and hydroxyl groups on catalyst surface. The roles of surface hydroxyl groups will be discussed in details in Section 4.2.

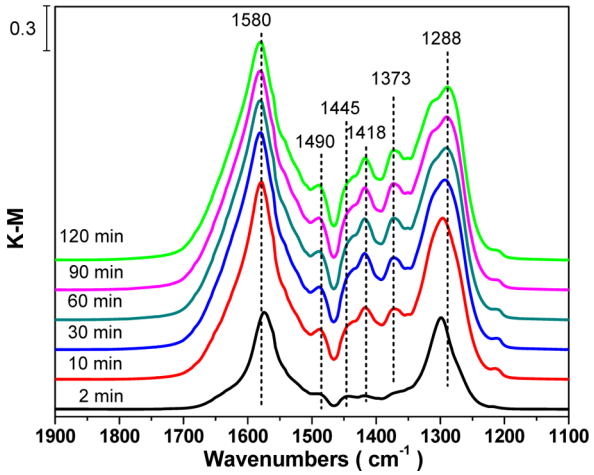

Figure 5. In situ DRIFT spectra of CO adsorption on Au/CeO_2 catalyst at 20 °C, under conditions of 2000 ppm of CO balance He stream, 100 mL·min^{-1} of flow rate.

Table 2. DRIFTS Band Position of Surface Species on CeO_2 and Au/CeO_2 Catalyst

species	catalyst	wavenumbers (cm^{-1})	ref
$[COOH]_s$	Au/CeO_2	1588, 1374	45
	Au/CeO_2	1575, 1375, 1358	10
	CeO_2	1580−1560, 1400−1350	46
	CeO_2	1560, 1410	48
monodentate carbonate	CeO_2	1480−1460, 1380−1360	46
	CeO_2	1454, 1354	48
	$Au/CePO_4$	1504, 1351	47
bidentate carbonate	CeO_2	1310−1250	46
	Au/CeO_2	1291	45
	Au/CeO_2	1276	10
	$Au/CePO_4$	1289	47
water	Au/CeO_2	1648	10
	$Au/CePO_4$	1630	47

Figure 6A,B show the change in band intensity of surface species over Au/CeO_2 catalysts with TOS under dry and wet conditions. Upon exposure to CO in dry stream, the bands attributed to $[COOH]_s$, monodentate, and bidentate carbonate species were observed. The band intensity of $[COOH]_s$ at 1576 cm^{-1} increased with time and became stable after 200 min. For surface monodentate (1490, 1447 cm^{-1}) and bidentate carbonate (1279 cm^{-1}) species, their band intensities rapidly increased in the first 50 min, and then only increased slightly with additional time on stream. In contrast, as shown in Figure 6B, it took only 40 min to reach steady band intensity of $[COOH]_s$ at 1576 cm^{-1} under wet stream (versus 200 min in dry stream). Figure 6C plots the change in band intensity of $\nu_{as}(OCO)$ at 1576 cm^{-1} with time on stream. Clearly, $[COOH]_s$ formed much faster in wet stream than in dry stream. A slow accumulation of monodentate carbonate species (1490, 1440 cm^{-1}) was also observed in the presence of water. The intensity of bidentate carbonate species at 1290 cm^{-1} reached a maximum at 10 min and decreased gradually thereafter, which indicates that water may facilitate the decomposition of bidentate carbonate species. It suggested that the monodentate and bidentate carbonate species on Au/CeO_2 catalysts slowly accumulated with TOS under dry stream, while only that of the monodentate carbonate species slowly accumulated under wet stream.

3.3.2. Consumption of Intermediates. Figure 7 shows the consumption of $[COOH]_s$ in various streams measured by in situ DRIFTS. The Au/CeO_2 catalyst was initially exposed to a standard stream containing 2000 ppm of CO, 20 vol % O_2 balance He at 20 °C for 220 min (CO/O_2/He, blue curve). After that, it was exposed to three types of streams: (1) pure

dx.doi.org/10.1021/cs500614f | ACS Catal. 2014, 4, 3481−3489

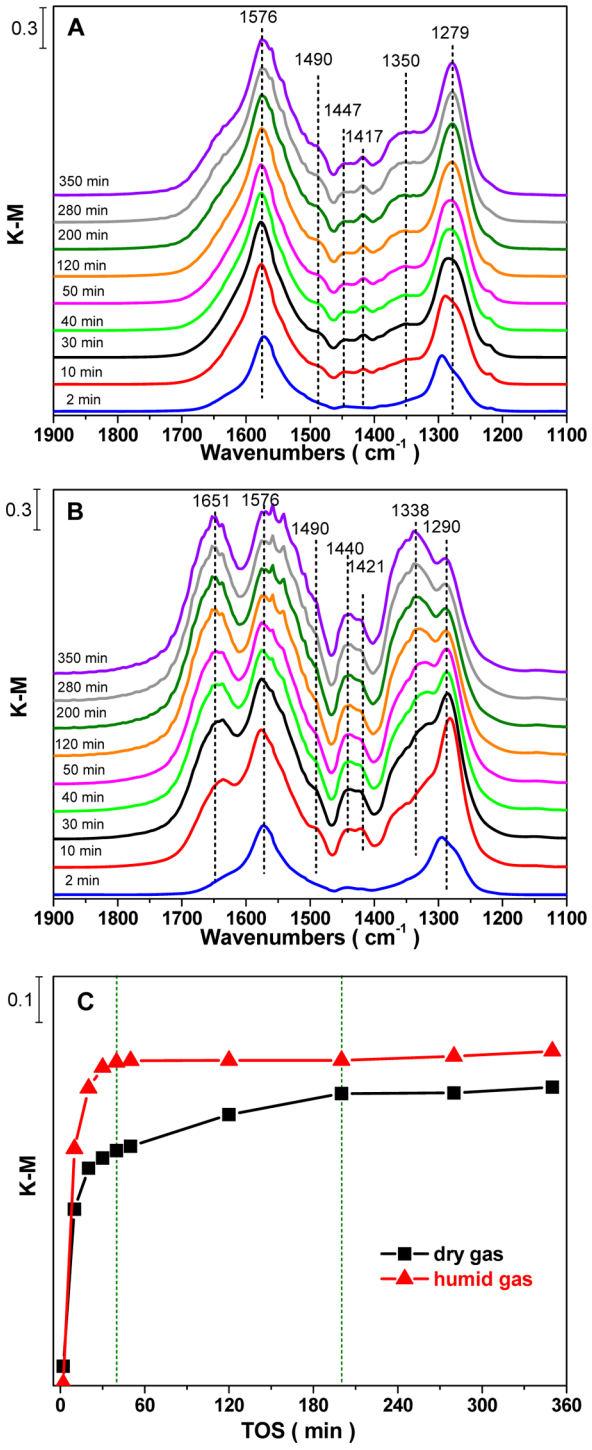

Figure 6. In situ DRIFT spectra of CO oxidation on Au/CeO_2 catalyst under (A) dry stream, (B) wet stream in the presence of 0.74 vol % H_2O, and (C) band intensity at 1576 cm^{-1} versus time under 2000 ppm of CO and 20 vol % O_2 balance He, at a flow rate of 100 mL·min^{-1}.

helium (He, red curve), (2) 20 vol % O_2 balance helium (O_2/He, black curve), and (3) 20 vol % O_2 and 0.74 vol % H_2O balance helium (O_2/H_2O/He, olive curve). In order to determine the consumption rate of $[COOH]_s$, the bands at 1800−1460 cm^{-1} were resolved into three peaks. Compared with the initial DRIFTS spectra under standard stream after 220 min of CO oxidation, the band intensity of $[COOH]_s$ at

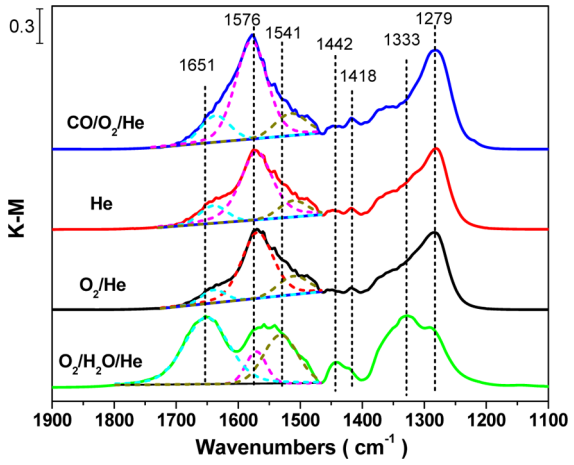

Figure 7. In situ DRIFT spectra of $[COOH]_s$ consumption on Au/CeO_2 catalyst under various streams after its exposure to 2000 ppm of CO, 20 vol % O_2 balance He for 220 min.

1576 cm^{-1} decreased in all three types of streams mentioned above. The highest decrease was observed with the wet stream (O_2/H_2O/He), which implies the fastest consumption or removal of surface $[COOH]_s$ species. As listed in Table 3, the

Table 3. Consumption Rate of $[COOH]_s$ on Au/CeO_2 Catalyst under Various Streams

atmosphere	He	20 vol % O_2/He	20 vol % O_2/0.74 vol % H_2O/He
rate[a]	0.22	0.31	0.81

[a]The consuming rate of $[COOH]_s$ species can be determined based on the kinetic dependence of DRIFTS band intensity of $[COOH]_s$. The rate was defined as rate = $\Delta I/\Delta t$ (ΔI: refers to the change in band intensity at 1576 cm^{-1} attributed to ν_{as}(OCO) of $[COOH]_s$; Δt: refers to the reaction time of 60 min).

consumption rate of $[COOH]_s$ species increased in the following order: He < O_2/He < O_2/H_2O/He. Clearly, the presence of H_2O and O_2 could facilitate the removal of $[COOH]_s$ intermediates. Compared to the initial standard stream containing CO, the band intensities at 1541, 1490, 1442, 1418, and 1333 cm^{-1} did not change significantly or just increased slightly in the three CO-free streams, which in part, might be ascribed to $[COOH]_s$ conversion into stable carbonates species. However, it should be noted that the peak at 1576 cm^{-1} assigned to ν_{as}(OCO) of $[COOH]_s$ is the main band of $[COOH]_s$. The bands at 1373 and 1418 cm^{-1} are also related to ν_s(OCO) and δ(OH) of $[COOH]_s$, possibly with some contributions from monodentate carbonate species.[39,48] Although the band at 1576 cm^{-1} is associated with those at 1373 and 1418 cm^{-1}, those two last bands did not decrease in the same way as the first one.

4. DISCUSSION

4.1. Physicochemical Properties of Au/CeO_2 Catalyst.

Induction period for CO oxidation has been previously observed and reported over certain Au-containing systems.[49−54]

To the best of our knowledge, there were no reports concerning induction period and humidity effect of CO oxidation over, in particular, Au/CeO_2 catalysts. Herein, Au/CeO_2 catalyst prepared by the deposition−precipitation method with urea was investigated in an effort to discover

dx.doi.org/10.1021/cs500614f | ACS Catal. 2014, 4, 3481−3489

the existence of induction period during CO oxidation at room temperature.

H_2-TPR and XPS techniques were used to characterize the physicochemical properties of the Au/CeO_2 samples. The redox properties of ceria were greatly modified after loading with Au. It suggests that the presence of gold facilitates activation (dissociation) of hydrogen molecules on metallic gold particles and leads to the migration of the dissociated hydrogen species by spillover process from the Au particles to the support.[42] However, when the catalyst contains ionic gold, the surface oxygen reducibility could be intensified through the lattice substitution mechanism, as reported by Fu et al.[55] In this case, the interaction of Au with ceria weakens the strength of surface Ce−O bonds adjacent to gold atoms, leading to a higher surface oxygen mobility.[55−57] The existence of cationic gold is confirmed in this work by XPS measurements (see Figure 1 and Table 1), indicating the presence of a strong metal interaction with support. However, the cationic Au species undergoes in situ reduction to metallic Au during CO oxidation in both dry and wet streams.[50−54] After CO oxidation in wet stream, the proportion of metallic Au is higher than in dry stream, which suggests that the presence of water accelerates the reduction of cationic Au, as reported previously.[53,54,58] The role of water on reducing cationic Au may be related to its electron-donation capability.[59] The lone electron pair on the water molecule can be donated to the π orbital of Au. This electron donation effect keeps Au electron-rich and from being oxidized.

4.2. Mechanism for Induction Period and Humidity Effect. Evidenced by the formation of $[COOH]_s$ species even in the absence of water and O_2 (see Figure 5), it is proposed that CO directly reacts with surface hydroxyl groups on Au/CeO_2 catalyst to form $[COOH]_s$ intermediates via R1

$$CO(ad) + [OH]_s \xrightarrow{k_1} [COOH]_s \quad (R1)$$

According to R1, an abundance of surface hydroxyl groups can promote the production of $[COOH]_s$ intermediates, whereas water vapor in humid stream can help to generate more hydroxyl groups via R2[60−62]

$$O_2 + H_2O \rightarrow [O]_s + 2OH \quad (R2)$$

Therefore, the extra surface hydroxyl groups generated on Au/CeO_2 catalyst under wet stream facilitate the formation of $[COOH]_s$ intermediates and thus shorten the induction period and enhance the initial activity.

DRIFTS measurements were conducted to further investigate the humidity effect on the consumption of $[COOH]_s$ intermediates. As shown in Figure 7, $[COOH]_s$ species were rapidly consumed in the presence of O_2 and H_2O. The $[COOH]_s$ consumption rate in the presence of water was nearly 4-fold of that in pure helium, suggesting that water promotes a complete oxidation of $[COOH]_s$ species into CO_2 via R3[63] and R4

$$[COOH]_s + [OH]_s \xrightarrow{k_2} CO_2 + H_2O \quad (R3)$$

$$[COOH]_s + [O]_s \xrightarrow{k_3} CO_2 + [OH]_s \quad (R4)$$

Generally, hydroxyl groups are associated with CeO_2, but some hydroxyl groups may exist on the edge of gold nanoparticles or near the interface between gold and support, which may contribute more to R1 and R3 reactions than the hydroxyl groups on the support. Worth noting is that water not only promotes the formation of $[COOH]s$ species but also helps to transform Au^+ and Au^{3+} species into metallic Au. These two effects are coupled and dependent for the target reaction.

According to a previous work on Au/CeO_2 catalysts prepared with the same method as in this work (deposition-precipitation with urea), Au is still in the oxidation state III in a sample containing 1 wt % Au after calcination, in contrast to Au on alumina or on titania.[64] However, the authors did mention that XPS analysis induced reduction of part of the gold,[65] suggesting that gold particles can be easily reduced at certain conditions. The sample color of our Au/CeO_2 catalyst is gray after calcination in synthetic air at 300 °C, which indicates that cationic gold was partially reduced to metallic gold, in agreement with the observations reported by Delannoy et al.[64]

The induction period of our Au/CeO_2 catalyst is considered to arise from unreduced cationic Au. The reduction of unreduced cationic Au can be promoted by water during CO oxidation, hence the induction period is significantly shortened in the presence of water. In addition, the length of induction period is in line with our observation of $[COOH]_s$ formation during CO oxidation with in situ DRIFTS. The induction period related to the unreduced cationic Au has been observed in some other catalysts such as Au/SiO_2 and Au/ZrO_2.[50,52−54] In situ reduction of the cationic Au during CO oxidation generates metallic Au species that are active for CO oxidation.[52−54] Addition of H_2O to the feed gas shortened the induction period of CO oxidation, due to a rapid reduction in cationic Au promoted by water.[54] In this work, $[COOH]_s$ formation correlated with the induction period, as indicated by the change in band intensity of $[COOH]_s$ at 1576 cm^{-1} with time (see Figure 6). However, the saturation of $[COOH]_s$ formation (see Figure 6C) takes longer than the induction period shown in Figure 3. This difference is related to the experimental setup of our reaction apparatus and DRIFTS cell. For activity measurement, catalyst pellets were loosely packed in the U-tube quartz reactor, which allowed gas passing through the catalyst bed easily with no diffusion limitation. However, for DRIFTS experiments, the catalyst was packed in the DRIFTS cell to form a flat surface. The feed gas could only readily adsorb on the surface but it took much longer for CO, water and O_2 to diffuse into the bulk to form active surface species. Therefore, it is not surprising to observe longer induction period with in situ DRIFTS than with activity measurements.

As illustrated in Figure 8, a mechanism is proposed to explain the induction period of Au/CeO_2, which involves reaction of adsorbed CO with formed surface $[COOH]_s$ species in both dry and wet streams. Because there are plenty of surface Au^+ and Au^{3+} species in the Au/CeO_2 catalyst, as evidenced by XPS data, it is likely that some OH groups are associated with surface Au^+ and Au^{3+} species. Before exposure to reactant stream, a few hydroxyl groups exist on catalyst surface. Under dry air stream, the surface hydroxyl groups on CeO_2 support slowly migrate to active sites near gold nanoparticles driven by the formation of $[COOH]_s$. As a consequence, a long induction period is needed under dry condition to reach maximum CO conversion. However, in wet stream, there are plenty of surface hydroxyl groups generated via R2 on the active sites near gold nanoparticles, which lead to a significantly short induction period, as shown in Figure 4B. In short, in terms of its effect on induction period and catalytic activity during induction and deactivation periods, humidity contributes to rapid formation of hydroxyl groups and $[COOH]_s$ intermediates near catalyst

dx.doi.org/10.1021/cs500614f | ACS Catal. 2014, 4, 3481−3489

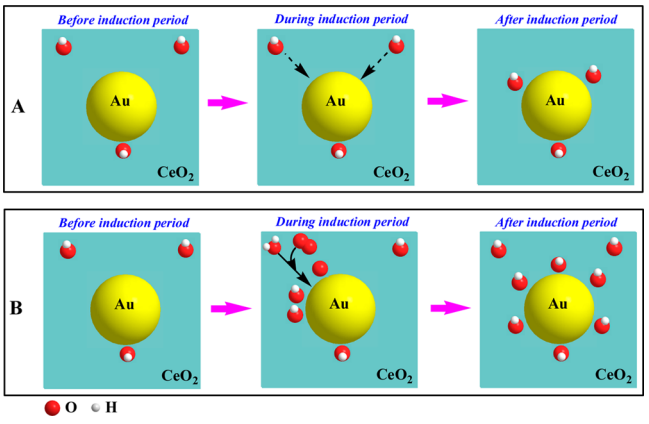

Figure 8. Schematic diagram of proposed mechanism for induction period under (A) dry stream and (B) wet stream.

surface, and to the consumption of $[COOH]_s$ intermediates, via R3 and R4.

For deactivation, there were two stages in wet stream, including an initial fast deactivation followed by a slow deactivation. However, in dry stream, only slow deactivation was observed, as shown in Figure 3. The fast deactivation in wet stream is ascribed to the blockage of active sites by water. There are three possible explanations for the slight deactivation, that is, aggregation of Au particles, change in chemical state of Au species, and accumulation of carbonate species. In the literature,[24,44,51−53,60] there was no significant change in particle size after CO oxidation over various Au catalysts, including catalysts used in wet streams.[44,60] Takeda et al. reported the reconstruction of (100) facet of gold nanoparticle supported on CeO_2 during CO oxidation at room temperature.[66,67] Figure S3 exhibits the HRTEM image and statistic analysis of Au particles on our Au/CeO_2 catalyst. Based on the HRTEM observations, the mean size of Au particles was around 3 nm before reaction, after induction period, and after reaction. Because CO concentration in feed gas was only around 500 ppm, and the reactor was surrounded by water bath, temperature increase in catalyst bed arising from the exothermic oxidation reaction was negligible, and thus had no contribution to catalyst particle sintering. This is in line with observations in literatures that no obvious change in the size of gold nanoparticles after reaction.[24,44,51−53,60] Therefore, the induction period of CO oxidation over Au/CeO_2 is related to unreduced cationic Au, without any contribution from particle size effect. Consistent with the proposed mechanism, more Au^0 species were formed in wet stream than in dry stream.

Carbonate species were observed with in situ DRIFTS measurement (Figure 6). As the reaction proceeded, the band intensity ascribed to carbonated species increased. Therefore, it can be deduced that catalyst deactivation is closely related to the buildup of carbonate species, which blocks active sites for CO oxidation, in agreement with recent findings.[18−22]

4.3. Humidity Effect Coorelated with Catalyst Support. Humidity affects CO oxidation differently over Au catalysts supported on different metal oxides. Over Au/ZrO_2 catalyst, moisture addition to the gaseous feed of the CO oxidation reaction eliminates the induction period.[54] In addition, over Au/Fe_2O_3 and Au/Al_2O_3 catalysts, a positive effect of humidity on alleviated activity loss was observed,[18,19] although over Au/TiO_2 and $Au/In_2O_3−TiO_2$ catalysts, a negative effect of humidity on catalyst deactivation was observed due to loss of active sites.[13,23] Humidity effect on our Au/CeO_2 catalyst is similar to that on some supported Au catalysts such as Au/ZrO_2.[54] For our Au/CeO_2 catalyst, induction period was significantly reduced from 44.8 min in dry air stream to 2.0−3.3 min in wet stream containing 0.58 to 0.97 vol % of H_2O. In summary, in wet stream, the Au/CeO_2 catalyst showed higher initial activity, significantly shorter induction period, but faster deactivation rate than in dry stream.

5. CONCLUSIONS

Induction period caused by unreduced cationic Au was discovered during CO oxidation at room temperature over Au/CeO_2 catalyst. The effect of humidity on catalyst activity was investigated during induction and deactivation periods. Moisture is crucial on CO oxidation with respect to the induction period, initial activity, and deactivation rate of Au/CeO_2 catalyst. In particular, the induction period was significantly reduced from 44.8 min in dry stream to 2.0−3.3 min with wet stream containing 0.58 to 0.97 vol % of H_2O. The highest initial activity was achieved in the presence of ~0.74 vol % H_2O. Humidity promoted the formation and consumption of $[COOH]_s$ intermediates, and thus enhanced initial activity, as evidenced by in situ DRIFTS measurements. Deactivation of Au/CeO_2 catalyst was observed under both dry and wet streams. In dry stream, only slow deactivation was observed. However, in wet stream, the catalyst first showed a rapid deactivation after the induction period and then underwent a slow deactivation stage. The rapid deactivation in wet stream is attributed to rapid blockage of active sites by adsorbed water, although the slow deactivation is related to gradual buildup of carbonate species on catalyst surface.

■ ASSOCIATED CONTENT

Supporting Information

DRIFT spectrum of Au/CeO_2 catalyst (Figure S1), CO-TPSR profiles of Au/CeO_2 (Figure S2) and HRTEM image of fresh Au/CeO_2 catalyst (Figure S3). This material is available free of charge via the Internet at http://pubs.acs.org.

■ AUTHOR INFORMATION

Corresponding Authors

*E-mail: xzhu@dlut.edu.cn. Tel./Fax: +86-411-84706094 (X.Z.).

*E-mail: chuanshi@dlut.edu.cn. Tel./Fax: +86-411-84986083 (C.S.).

Notes

The authors declare no competing financial interest.

■ ACKNOWLEDGMENTS

This work is supported by National Natural Science Foundation of China (11175036, U1201231) and the Fundamental Research Funds for the Central Universities (DUT14RC(3)012).

■ REFERENCES

(1) Akita, T.; Lu, P.; Ichikawa, S.; Tanaka, K.; Haruta, M. *Surf. Interface Anal.* **2001**, *31*, 73−78.

(2) Overbury, S. H.; Schwartz, V.; Mullins, D. R.; Yan, W.; Dai, S. *J. Catal.* **2006**, *241*, 56−65.

(3) Zanella, R.; Louis, C. *Catal. Today* **2005**, *107−108*, 768−777.

(4) Bokhimi, X.; Zanella, R.; Morales, A.; Maturano, V.; Ángeles-Chávez, C. *J. Phys. Chem. C* **2011**, *115*, 5856−5862.

(5) Azar, M.; Caps, V.; Morfin, F.; Rousset, J.-L.; Piednoir, A.; Bertolini, J.-C.; Piccolo, L. *J. Catal.* **2006**, *239*, 307−312.
(6) Park, E. D.; Lee, J. S. *J. Catal.* **1999**, *186*, 1−11.
(7) Avgouropoulos, G.; Ioannides, T.; Papadopoulou, Ch.; Batista, J.; Hocevar, S.; Matralis, H. K. *Catal. Today* **2002**, *75*, 157−167.
(8) Neri, G.; Bonavita, A.; Rizzo, G.; Galvagno, S.; Donato, N.; Caputi, L. S. *Sens. Actuators, B* **2004**, *101*, 90−96.
(9) Romero-Sarria, F.; Penkova, A.; Martinez, T. L. M.; Centeno, M. A.; Hadjiivanov, K.; Odriozola, J. A. *Appl. Catal., B* **2008**, *84*, 119−124.
(10) Chen, B.-B.; Shi, C.; Crocker, M.; Wang, Y.; Zhu, A.-M. *Appl. Catal., B* **2013**, *132*−*133*, 245−255.
(11) Costello, C. K.; Kung, M. C.; Oh, H.-S.; Wang, Y.; Kung, H. H. *Appl. Catal. A: Gen.* **2002**, *232*, 159−168.
(12) Diemant, T.; Bansmann, J.; Behm, R. J. *Vacuum* **2010**, *84*, 193−196.
(13) Debeila, M. A.; Wells, R. P. K.; Anderson, J. A. *J. Catal.* **2006**, *239*, 162−172.
(14) Olea, M.; Tada, M.; Iwasawa, Y. *J. Catal.* **2007**, *248*, 60−67.
(15) Schumacher, B.; Plzak, V.; Kinne, M.; Behm, R. J. *Catal. Lett.* **2003**, *89*, 109−114.
(16) Lee, W.-S.; Wan, B.-Z.; Kuo, C.-N.; Lee, W.-C.; Cheng, S. *Catal. Commun.* **2007**, *8*, 1604−1608.
(17) Wu, Y.; Sun, K.-Q.; Yu, J.; Xu, B.-Q. *Phys. Chem. Chem. Phys.* **2008**, *10*, 6399−6404.
(18) Schubert, M. M.; Venugopal, A.; Kahlich, M. J.; Plzak, V.; Behm, R. J. *J. Catal.* **2004**, *222*, 32−40.
(19) Kung, H. H.; Kung, M. C.; Costello, C. K. *J. Catal.* **2003**, *216*, 425−432.
(20) Bollinger, M. A.; Vannice, M. A. *Appl. Catal., B* **1996**, *8*, 417−443.
(21) Konova, P.; Naydenov, A.; Venkov, Cv.; Mehandjiev, D.; Andreeva, D.; Tabakova, T. *J. Mol. Catal. A: Chem.* **2004**, *213*, 235−240.
(22) Denkwitz, Y.; Schumacher, B.; Kučerová, G.; Behm, R. J. *J. Catal.* **2009**, *267*, 78−88.
(23) Grunwaldt, J.-D.; Kiener, C.; Wögerbauer, C.; Baiker, A. *J. Catal.* **1999**, *181*, 223−232.
(24) Fan, H.-Y.; Shi, C.; Li, X.-S.; Zhang, S.; Liu, J.-L.; Zhu, A.-M. *Appl. Catal., B* **2012**, *119*−*120*, 49−55.
(25) Epling, W. S.; Hoflund, G. B.; Weaver, J. F.; Tsubota, S.; Haruta, M. *J. Phys. Chem.* **1996**, *100*, 9929−9934.
(26) Liu, Y.; Liu, B.; Wang, Q.; Li, C.; Hu, W.; Liu, Y.; Jing, P.; Zhao, W.; Zhang, J. *J. Catal.* **2012**, *296*, 65−76.
(27) Abd El-Moemen, A.; Karpenko, A.; Denkwitz, Y.; Behm, R. J. *J. Power Sources* **2009**, *190*, 64−75.
(28) Camellone, M. F.; Fabris, S. *J. Am. Chem. Soc.* **2009**, *131*, 10473−10483.
(29) Tabakova, T.; Manzoli, M.; Vindigni, F.; Idakiev, V.; Boccuzzi, F. *J. Phys. Chem. A* **2010**, *114*, 3909−3915.
(30) Longo, A.; Liotta, L. F.; Pantaleo, G.; Giannici, F.; Venezia, A. M.; Martorana, A. *J. Phys. Chem. C* **2012**, *116*, 2960−2966.
(31) Minicò, S.; Scirè, S.; Crisafulli, C.; Galvagno, S. *Appl. Catal., B* **2001**, *34*, 277−285.
(32) Guzman, J.; Carrettin, S.; Corma, A. *J. Am. Chem. Soc.* **2005**, *127*, 3286−3287.
(33) Pillai, U. R.; Deevi, S. *Appl. Catal., A* **2006**, *299*, 266−273.
(34) Han, M.; Wang, X.; Shen, Y.; Tang, C.; Li, G.; Smith, R. L. *J. Phys. Chem. C* **2010**, *114*, 793−798.
(35) Carabineiro, S. A. C.; Silva, A. M. T.; Dražić, G.; Tavares, P. B.; Figueiredo, J. L. *Catal. Today* **2010**, *154*, 21−30.
(36) Ying, F.; Wang, S.; Au, C.-T.; Lai, S.-Y. *Gold Bull.* **2010**, *43*, 241−251.
(37) Shen, B.; Liu, T.; Zhao, N.; Yang, X.; Deng, L. *J. Environ. Sci.* **2010**, *22*, 1447−1454.
(38) Cheng, D.-G.; Chong, M.; Chen, F.; Zhan, X. *Catal. Lett.* **2008**, *120*, 82−85.
(39) Jin, T.; Zhou, Y.; Mains, G. J.; White, J. M. *J. Phys. Chem.* **1987**, *91*, 5931−5937.
(40) Kondarides, D. I.; Verykios, X. E. *J. Catal.* **1998**, *174*, 52−64.
(41) Shyu, J. Z.; Otto, K.; Watkins, W. L. H.; Graham, G. W.; Belitz, R. K.; Gandhi, H. S. *J. Catal.* **1988**, *114*, 23−33.
(42) Dobrosz-Gómez, I.; Kocemba, I.; Rynkowski, J. M. *Catal. Lett.* **2009**, *128*, 297−306.
(43) Shyu, J. Z.; Weber, W. H.; Gandhi, H. S. *J. Phys. Chem.* **1988**, *92*, 4964−4970.
(44) Daté, M.; Haruta, M. *J. Catal.* **2001**, *201*, 221−224.
(45) Denkwitz, Y.; Karpenko, A.; Plzak, V.; Leppelt, R.; Schumacher, B.; Behm, R. J. *J. Catal.* **2007**, *246*, 74−90.
(46) Bozon-Verduraz, F.; Bensalem, A. *J. Chem. Soc., Faraday Trans.* **1994**, *90*, 653−657.
(47) Romero-Sarria, F.; Domínguez, M. I.; Centeno, M. A.; Odriozola, J. A. *Appl. Catal., B* **2011**, *107*, 268−273.
(48) Appel, L. G.; Eon, J. G.; Schmal, M. *Catal. Lett.* **1998**, *56*, 199−202.
(49) Lin, J.-N.; Chen, J.-H.; Hsiao, C.-Y.; Kang, Y.-M.; Wan, B.-Z. *Appl. Catal., B* **2002**, *36*, 19−29.
(50) Boyd, D.; Golunski, S.; Hearne, G. R.; Magadzu, T.; Mallick, K.; Raphulu, M. C.; Venugopal, A.; Scurrell, M. S. *Appl. Catal., A* **2005**, *292*, 76−81.
(51) Yang, J. H.; Henao, J. D.; Raphulu, M. C.; Wang, Y.; Caputo, T.; Groszek, A. J.; Kung, M. C.; Scurrell, M. S.; Miller, J. T.; Kung, H. H. *J. Phys. Chem. B* **2005**, *109*, 10319−10326.
(52) Wu, Z.; Zhou, S.; Zhu, H.; Dai, S.; Overbury, S. H. *Chem. Commun.* **2008**, 3308−3310.
(53) Wu, Z.; Zhou, S.; Zhu, H.; Dai, S.; Overbury, S. H. *J. Phys. Chem. C* **2009**, *113*, 3726−3734.
(54) Hong, Y.-C.; Sun, K.-Q.; Han, K.-H.; Liu, G.; Xu, B.-Q. *Catal. Today* **2010**, *158*, 415−422.
(55) Fu, Q.; Saltsburg, H.; Flytzani-Stephanopoulos, M. *Science* **2003**, *301*, 935−938.
(56) Scirè, S.; Minicò, S.; Crisafulli, C.; Satriano, C.; Pistone, A. *Appl. Catal., B* **2003**, *40*, 43−49.
(57) Fu, Q.; Weber, A.; Flytzani-Stephanopoulos, M. *Catal. Lett.* **2001**, *77*, 87−95.
(58) Boccuzzi, F.; Chiorino, A.; Tsubota, S.; Haruta, M. *J. Phys. Chem.* **1996**, *100*, 3625−3631.
(59) Baird, A. S.; Kross, K. M.; Gottschalk, D.; Hinson, E. A.; Wood, N.; Layman, K. A. *J. Phys. Chem. C* **2007**, *111*, 14207−14214.
(60) Daté, M.; Okumura, M.; Tsubota, S.; Haruta, M. *Angew. Chem., Int. Ed.* **2004**, *43*, 2129−2132.
(61) Boccuzzi, F.; Chiorino, A.; Manzoli, M.; Lu, P.; Akita, T.; Ichikawa, S.; Haruta, M. *J. Catal.* **2001**, *202*, 256−267.
(62) Zheng, Z.; Teo, J.; Chen, X.; Liu, H.; Yuan, Y.; Waclawik, E. R.; Zhong, Z.; Zhu, H. *Chem.—Eur. J.* **2010**, *16*, 1202−1211.
(63) Wang, H.-F.; Kavanagh, R.; Guo, Y.-L.; Guo, Y.; Lu, G.-Z.; Hu, P. *Angew. Chem., Int. Ed.* **2012**, *51*, 6657−6661.
(64) Delannoy, L.; Weiher, N.; Tsapatsaris, N.; Beesley, A. M.; Nchari, L.; Schroeder, S. L.M.; Louis, C. *Topics Catal.* **2007**, *44*, 263−273.
(65) Lakshmanan, P.; Delannoy, L.; Richard, V.; Méthivier, C.; Potvin, C.; Louis, C. *Appl. Catal., B* **2010**, *96*, 117−125.
(66) Yoshida, H.; Kuwauchi, Y.; Jinschek, J. R.; Sun, K.; Tanaka, S.; Kohyama, M.; Shimada, S.; Haruta, M.; Takeda, S. *Science* **2012**, *335*, 317−319.
(67) Zhu, Y.; Zhang, S.; Shan, J.; Nguyen, L.; Zhan, S.; Gu, X.; Tao, F. *ACS Catal.* **2013**, *3*, 2627−2639.